Am J Cancer Res 2022;12(3):1264-1281
www.ajcr.us /ISSN:2156-6976/ajcr0133911

Original Article

RP11-867G2.8 promotes EMT and chordoma malignant phenotypes by enhancing FUT4 mRNA stability and translation

Ming Yang, Shi Chang Liu, Ding Jun Hao, Liang Yan, Zhong Kai Liu, Xin Hua Yin

Department of Spine Surgery, Hong Hui Hospital, Xi'an Jiaotong University College of Medicine, Xi'an, Shaanxi, China

Received April 4, 2021; Accepted February 23, 2022; Epub March 15, 2022; Published March 30, 2022

Abstract: Chordoma is a rare bone tumor, and the recurrence rate of chordoma is high, the treatment is difficult, and the prognosis is poor. Therefore, it is of great significance to find key target genes for the treatment of chordoma. Microarray was used to analyze the significant gene associated with chordoma. Western blot and RT-PCR were used to detect protein and mRNA expression levels of RP11-867G2.8 and FUT4. Fluorescence in situ hybridization (FISH) assay was used to locate the position of RP11-867G2.8 in chordoma cells. MTT assay, colony formation assay, transwell assay and Xenograft Mouse Model were used to clarify the function of RP11-867G2.8 and FUT4. RNA pull-down, RNA immunoprecipitation, RNA stability assay and polysome profiling analysis were used to clarify the relationship between RP11-867G2.8 and FUT4. We found that RP11-867G2.8 is highly expressed in chordoma tissues and cells, and RP11-867G2.8 overexpression promotes the malignant biological behavior of chordoma cells. RP11-867G2.8 overexpression alters the expression pattern of genes modulating signaling pathway. FUT4 is accumulated in chordoma tissues, and RP11-867G2.8 is antisense RNA of FUT4. RP11-867G2.8 can bind to FUT4 mRNA, increasing FUT4 mRNA stability and facilitating translation of FUT4. RP11-867G2.8 binds to EIF4B and PABPC1, which increases the translation of FUT4. Further studies found that FUT4 silence counteracts the effect of RP11-867G2.8 *in vivo* and *in vitro*. Our results suggest that RP11-867G2.8 promotes the development and progression of chordoma by up-regulating the expression of FUT4.

Keywords: RP11-867G2.8, long non-coding RNA, chordoma, EMT, FUT4

Introduction

Chordoma is a rare bone tumor that accounts for about 2% to 4% of all bone tumors [1-3]. It mainly originates from embryonic notochord cells and occurs in the humerus and the skull base [4]. Nowadays, surgical resection is the main therapy for chordoma because it is insensitive to chemotherapy and radiotherapy [5]. Given that chordoma has a high invasive ability and recurrence rate, the treatment is difficult and the prognosis is poor [6, 7]. In view of the single treatment and poor efficacy of chordoma, studying the occurrence and development of chordoma will help us better understand the disease and develop related molecular targeted drugs.

Long non-coding RNAs (lncRNAs) are a class of transcription products that are >200 bases in length. LncRNAs do not encode proteins while encode a small number of short peptides [8]. Many studies have shown that lncRNAs can participate in the regulation of a variety of malignant processes, including cell proliferation, metastasis, invasion, apoptosis and autophagy, as well as participate in tumor radio-chemotherapy resistance [9-12]. So far, studies have confirmed that lncRNAs act as oncogenes and tumor suppressors in malignant tumors [13-15]. However, the underlying mechanisms have not been extensively elucidated. In chordoma, studies showed that long non-coding RNA LOC554202 modulates cell proliferation and invasion by recruiting EZH2 and regulating miR-31 expression [16]. The role of the imprinted gene cluster DLK1-MEG3 has been associated with mRNA-lncRNA co-expression profiles [17]. Therefore, it is of great clinical significance to

Table 1. The shRNA sequences

Names	shRNA numbers	Target Sequence
FUT4	shRNA1	CGCAGCACCTGGATTATATCA
	shRNA2	**CGCTGACTTCTTTCACAAGTA**
	shRNA3	CCTAAGGTTGAAAGTGCTTAT
EIF4B	shRNA1	**GCCGGGATATGGATCGATATG**
	shRNA2	TGGTAATGACAGTGATATAAT
	shRNA3	GCGGAGAAACACCTTGATCTT
PABPC1	shRNA1	**GGACAAATCCATTGATAATAA**
	shRNA2	AGCTGTTCCCAACCCTGTAAT
	shRNA3	GCAAACATAATGCTAGTCCTA
RP11-867G2.8	shRNA1	GAGGAAACTGAAGATAAAGCTAT
	shRNA2	AGGGTTACTACTGATATCACTGG
	shRNA3	**TGGGTGTTTGAAGAACTTACTCC**

The sequences marked with bold were used in the formal studies.

study the relationship between lncRNAs and the development of chordoma.

LncRNA RP11-867G2.8 (AP000943.4) is a non-protein-coding gene located on human chromosome 11. So far, no research has reported about the function and mechanism of RP11-867G2.8. In the present study, we also explored the specific mechanism of RP11-867G2.8 function. Fucosyltransferase 4 (FUT4) is a novel regulator of epithelial-mesenchymal transition (EMT), which is a crucial step in tumor progression [18]. In addition, researchers found that cancer-related CD15/FUT4 overexpression participates in cetuximab or bevacizumab mechanisms of resistance in metastatic colorectal cancer patients [19]. Although many studies reported FUT4 as an oncogene [20, 21], FUT4 has not been reported in chordoma so far.

In the present study, we found that RP11-867G2.8 is a natural antisense RNA of FUT4, and FUT4 is also low expressed in chordoma tissues. Overexpression of RP11-867G2.8 upregulated the expression level of FUT4. Therefore, we further explored whether RP11-876G2.8 promotes the malignant phenotype of chordoma and the specific mechanism by which RP11-867G2.8 modulates FUT4.

Materials and methods

Microarray analysis

Chordoma tissues and normal nucleus pulposus tissues were obtained from Hong Hui Hospital, Xi'an Jiaotong University College of Medicine (Xi'an, China). All patients participated in this research were diagnosed as Chordoma by two pathologists, and none of them received any radiotherapy or chemotherapy prior to surgery. Signed informed consent was obtained from each patient. The levels of mRNA and lncRNA expression in the tissues were analyzed using Human OneArray® v7 Microarrays (OneArray, Shanghai, China). Total RNA was extracted with the RNeasy Kit (Qiagen) to prepare the cyanine 3 (Cy3)-labeled complementary RNA (cRNA). The Cy3-labeled cRNA was fragmented and hybridized to the Human Microarray for 17 h. The slides were washed and scanned immediately on an Agilent DNA Microarray Scanner (G2565CA) using the one-color scan setting for 8×60 K array slides.

Cell lines and transfection

The chordoma cell lines U-CH1, U-CH2, U-CH7 and JHC7 were purchased from American Type Culture Collection (ATCC, Rockville, MD, USA). All cells were cultured in Dulbecco's modified Eagle's medium (DMEM) supplemented with 10% fetal bovine serum (FBS; Gibco, Grand Island, NY, USA), 100 U/mL penicillin, and 100 μg/mL streptomycin. The cells were incubated in a 5% CO_2 atmosphere at 37°C.

To induced the expression of RP11, we ligated RP11-867G2.8 full sequence (RP11), RP11-867G2.8 sequence overlapping with FUT4 mRNA (RP11-O), and RP11-867G2.8 sequence non-overlapping with FUT4 (RP11-NO) into pcDNA™ 3.1 Mammalian expression vector (V79020, Invitrogen, Carlsbad, CA, USA) according to the manufacturer's instructions. Short-hairpin RNAs (shRNAs) were designed to down-regulate RP11-867G2.8, EIF4B, PABPC1, and FUT4 (**Table 1**). shRNAs were synthesized by GeneChem (Shanghai, China). Transfection was carried out using Lipofectamine™ 3000 Transfection Reagent (Invitrogen). In short, the cells were inoculated in 6-well plates and reached 70% confluence after 24 h. Then, the cells were transfected with DNA complexes using the transfection reagent according to the manufacturer's instructions.

Quantitative reverse-transcription PCR (qRT-PCR)

Total RNA was extracted from chordoma cells using Trizol reagent (Invitrogen). cDNA was amplified with the random primers and First Strand cDNA Synthesis Kit (Fermentas, Vilnius, Lithuania). β-actin was used as a housekeeping control. The forward and reverse primer sequences were as follows: RP11-867G2.8 5'-TGATGTGGACAGCGTAGCTC-3' and 5'-ACTCGCAGCACCTGGATTAT-3'; FUT4 5'-CTTCAACTGGACGCTCTCCTA-3' and 5'-GTTGGTGGTAGTAGCGGACC-3'; β-actin 5'-CATGTACGTTGCTATCCAGGC-3' and 5'-CTCCTTAATGTCACGCACGAT-3'. qRT-PCR was performed on 7300 Fast Real-time PCR system (Applied Biosystems, Foster City, CA, USA) using SYBR Green qPCR Mix (TOYOBO, Osaka, Japan). Relative expression was calculated according to the formula $2^{-\Delta\Delta CT}$.

Western blotting

Cells were washed with phosphate buffer saline (PBS) and then lysed with RIPA lysis buffer containing 10% protease inhibitor cocktail (Roche, Mannheim, Germany) on ice for 30 min. Protein concentrations were determined using a BCA Protein Assay Reagent kit (Thermo Scientific, Waltham, MA, USA). The proteins were separated using 12% SDS-PAGE and were electroblotted to a PVDF membrane (Millipore, Bedford, MA, USA). The membranes were blocked in 5% nonfat milk at 4°C overnight. Continually, the membranes were incubated with anti-FUT4 (1:500, 22141-1-AP, PTGCN, Wuhan, China), anti-vimentin (1:1000, 60330-1-Ig, PTGCN), anti-N-cadherin (1:1000, ab18203, Abcam, Cambridge, UK), anti-β-actin (1:2000, 3700S, CST, Danvers, MA, USA) for 2 hours, followed by incubation with the secondary antibody. Then, the bands were visualized using enhanced chemiluminescence. Band quantification was performed using Quantity One optical density analysis software (Bio-Rad, Hercules, CA, USA). GAPDH was used as an internal control to normalize the expression of the other proteins.

MTT assay

The U-CH1 and JHC7 cells were incubated in 96-well plates at a density of 5×10^3 cells/well in 100 μL of DMEM. After 72 h-incubation, 50 μL of MTT [3-(4,5-Dimethyl-2-thiazolyl)-2, 5-diphenyl-2Htetrazolium (Sigma)] was added to each well, and the cells were incubated for another 4 h. Subsequently, 150 μL dimethyl sulfoxide was added to each well to dissolve the crystals. The optical density of each well was then measured using microplate spectrophotometry at a wavelength of 570 nm.

Colony formation assay

After transfection, the cells (1,000 cells per well) were inoculated in culture dishes. A colony was defined to consist of at least 10 cells. Colonies were fixed with 4% paraformaldehyde, stained with Giemsa, and counted with the naked eye or using a stereomicroscope. The percentage of colonies formed was expressed as (number of colonies formed/number of cells seeded) ×100%.

Migration assay

To determine the migration capacity of the transfected U-CH1 and JHC7 cells, 24-well Transwell chambers with inserts (Corning, NY, USA) were used. A total of 5×10^4 cells in 200 μL of RPMI-1640/F-12 without FBS were loaded into the upper chamber of the Transwell. The lower chambers were added with 900 μL of the medium containing 5% FBS. The culture was maintained at 37°C in 5% CO_2 and 95% air. After a 24-h incubation, the non-migratory cells were removed using a cotton swab. Then the cells were fixed with 4% paraformaldehyde, stained with 0.1% crystal violet, and washed in PBS. The cells were observed and counted under an inverted microscope (Olympus, Tokyo, Japan).

RNA stability assay

To measure the stability of *FUT4* mRNA, 5 g/mL of actinomycin D (Sigma-Aldrich, St Louis, MO, USA) was added to the cell culture to inhibit transcription. RNA was harvested after incubation for 5 h, 10 h, and 15 h, and was subjected to qRT-PCR analysis for FUT4 expression at mRNA level. Transcript levels were plotted by appropriate nonlinear regression curves using a one-phase decay equation. RNA decay rate constant (k) was quantified by fitting an exponential curve to the data points (y = a*e-kt; y is the relative amount of RNA, and t is time). The turnover rate of mRNA was estimated according to previously pub-

lished paper [22]. The half-life was then estimated according to the equation t1/2 = ln(2)/k [23]. The normalizer transcript 18S rRNA that does not decay over the course of this experiment was detected as a control.

Polysome fractionation

Polysome fractionations were performed as described previously [24, 25]. Briefly, the cells (four 150-mm culture dishes) were treated with 100 ug/mL cycloheximide (Sigma-Aldrich) for 10 min at 37°C. Then, the cells were harvested and 1 mL of cytoplasmic extract was layered onto 11 mL of 10%-50% sucrose gradient and centrifuged at 36,000 rpm in a Beckman SW-41Ti rotor for 2.5 h at 4°C. Gradient fractionation was fractionated and continuously monitored at 254 nm using a density gradient fractionation system (Brandel, Gaithersburg, MD, USA). The collected fractions were then analyzed by Western blotting or qRT-PCR.

RNA pull-down assay

Bio (biotinylated)-NC, bio-RP11-867G2.8 overlap (RP11-O) and bio-RP11-867G2.8 non-overlap (RP11-NO), which were labelled with RNA Labeling Mix (Roche) *in vitro*, were transfected into U-CH1 and JHC7 cells, and the cell lysate was collected after 48 h. The cell lysate was combined with streptavidin-coupled magnetic bead (Invitrogen) to form a protein-bio/RNA-magnetic bead complex, and the protein-bio/RNA was obtained through high salt elution. The protein-bio/RNA was extracted and purified with TRIzol, and then FUT4 expression was detected using qRT-PCR as described above.

RNA immunoprecipitation-qRT-PCR

U-CH1 and JHC7 cells transfected with shRP11 were pelleted by centrifugation at 1000 g for 10 min at 4°C, followed by washing in pre-cold PBS three times. The cell pellets were lysed in an equal volume of polysome lysis buffer (100 mM KCl, 5 mM $MgCl_2$, 10 mM HEPES (pH 7.0), 0.5% NP40) in supplementation with 1 mM DTT, 100 per unit RNase (Invitrogen), 400 μM VRC, and protease inhibitor. The cell lysates were maintained on ice for 10 min. Protein A beads coated by antibodies against EIF4B, PABPC1 and IgG were prepared using the commercially available kit (Thermo Scientific) at 4°C. The antibody-coated beads were washed in pre-cold NT2 buffer before suspension in NT2 buffer containing 20 mM EDTA, 1 mM DTT, 400 μM vanadyl ribonucleosides complexes, and 200 units of an RNase inhibitor. After pre-incubation, the antibody coated beads were mixed with the cell lysate, and the mixture was incubated for 2 h at room temperature. The beads were washed in pre-cold NT2 buffer five times and washed in NT2 buffer containing 1% Triton X-100. RNAbee (Amsbio, Lake Forest, CA, USA) was used to extract RNA from the immunoprecipitated pellets. qRT-PCR was carried out for RP11-867G2.8 quantification as described above.

Fluorescence in situ hybridization (FISH) analysis

For FISH assay, fluorescence-conjugated lncRNA RP11-867G2.8 probes were generated according to the manual of Biosearch Technologies (Beijing, China). Chordoma cells were treated in a non-denaturing condition, followed by hybridization with lncRNA CASC2 probes. After RNA hybridization, samples were incubated in 4',6-diamidino-2-phenylindole (DAPI, 1:1000) for 5 min of counterstaining, and observed by a confocal microscopy (DMI4000B, Leica Microsystems, Nussloch, Germany). All experiments were performed according to the manuals of Biosearch Technologies.

Xenograft mouse model

All animal experiments were approved by the Animal Center of Central South University and performed following International Guidelines and Protocols. To generate tumors *in vivo*, 5×10^6 cells were injected subcutaneously into 4-week to 6-week old BALB/C nude mice on the right flank of their abdomen. When a tumor reached 100 mm^3 in volume, the tumor volume was measured every 3 day. After 30 days, the mouse was sacrificed and the tumors were isolated and measured using vernier calipers. The tumor volume was calculated using the following formula: tumor volume (in mm^3) = (the longest diameter × the shortest $diameter^2$)/2.

Immunohistochemistry

Cancer tissue sections were de-paraffinized and rehydrated with graded alcohols, then

treated with 0.3% H_2O_2 in methanol for 30 min and blocked with 1% PBA for 1 h. The prepared sections were incubated with antibody against Ki67 (Genetex, GTX16667) at 4°C overnight. The polymer enhancers were incubated at room temperature for 20 min and then biotin-labeled second antibody was added to incubate at room temperature for 30 min. Next, the sections were stained with a DAB staining solution and counterstained with hematoxylin and then mounted in glycerol-vinyl-alcohol (GVA) (Zymed, San Francisco, CA, USA). The score was determined by combining the proportion of positively stained tumor cells and the staining intensity.

Statistical analysis

GraphPad Prism 7.04 (GraphPad, San Diego, CA, USA) was used for all statistical analyses. All experiments were performed in triplicate. Data are expressed as the mean ± SD. Significance testing of data sets was conducted using analysis of variance followed by a comparison between the specific groups using the Student's t test, multiple comparison using Bonferroni's test and Tukey's test. $P<0.05$ in all cases was considered statistically significant.

Results

RP11-867G2.8 was highly expressed in chordoma tissues and cells and promoted the malignant biological behaviors of chordoma cells

We selected 3 cases of chordoma tissue and 3 cases of normal nucleus pulposus tissues to perform lncRNA array analysis (**Figure 1A**). All the data were shown in the Supplementary Table 1. A total of 285 lncRNAs were highly expressed in chordoma tissues ($P<0.05$ and fold changes >1). In the chordoma tissues seven highly expressed lncRNAs with fold changes more than 8 were selected for the further study (**Figure 1A**). We further tested the expression levels of these 7 lncRNAs in 12 pairs of chordoma tissues and normal nucleus pulposus tissues. Among all the lncRNAs, RP11-867G2.8 expression had the biggest increase in chordoma tissues compared to normal nucleus pulposus tissues ($P<0.001$, **Figure 1B**). Therefore, we chose RPGG-867G2.8 for further study. Subsequently, we selected U-CH1, U-CH2, U-CH7 and JHC7 cell lines derived from sacral chordoma cells, and we detected the expression level of RP11-867G2.8 by qRT-PCR. As shown in **Figure 1C**, U-CH1 and JHC7 cells showed high expression of RP11-867G2.8 compared with U-CH2 cells (both $P<0.001$). Continually, RP11-867G2.8 staining was performed in U-CH1 and JHC7 cells, and the representative images of fluorescence intensify demonstrated significant localization of RP11-867G2.8 in the cytoplasm and nucleus (**Figure 1D**).

To confirm RP11-867G2.8 (AP000943.4) is a non-coding RNA, we conducted a serious of analysis. Firstly, we used the Coding Potential Assessing Tool CPAT server (http://lilab.research.bcm.edu/) for the analysis. In detail, we used FUT4 and MALAT1 as the references of mRNA and lncRNA, respectively. The RNA sequences of RP11-867G2.8, FUT4 and MALAT1 were put into the Coding Potential Calculator (CPC) program. Results showed that the coding probability of FUT4 is very high, while the Coding Probability of RP11-867G2.8 and MALAT1 are very low (**Table 2**). Therefore, RP11-867G2.8 and MALAT1 were predicted to be non-coding RNAs, while FUT4 RNA was identified to code for protein. Moreover, we used another web for the analysis of the coding ability of RP11-867G2.8. PhyloCSF Candidate Coding Regions (https://github.com/mlin/PhyloCSF/wiki) is a web that uses comparative genomics method to distinguish protein coding region and non-coding region. Based on a formal statistical comparison of phylogenetic codon model, it analyzes a multi species nucleotide sequence alignment to determine whether it may represent a conserved protein coding region. The output value of PhyloCSF is more than zero, indicating a conservative coding area; otherwise, it indicates a non-coding area. As shown in Supplementary Figure 1A, the PhyloCSF values of RP11-867G2.8 and MALAT1 are less than zero, whereas the PhyloCSF value of FUT4 is more than zero. These results suggested that RP11-867G2.8 has no coding ability.

We designed three shRNAs to knock down RP11-867G2.8. As indicated by the PCR, the shRNA3 showed the strongest suppressive effect on RP11-867G2.8 expression, followed by the shRNA1 ($P<0.001$) (**Figure 1E**). Then, we investigated the role of RP11-867G2.8 in chordoma cells after knocking down RP11-

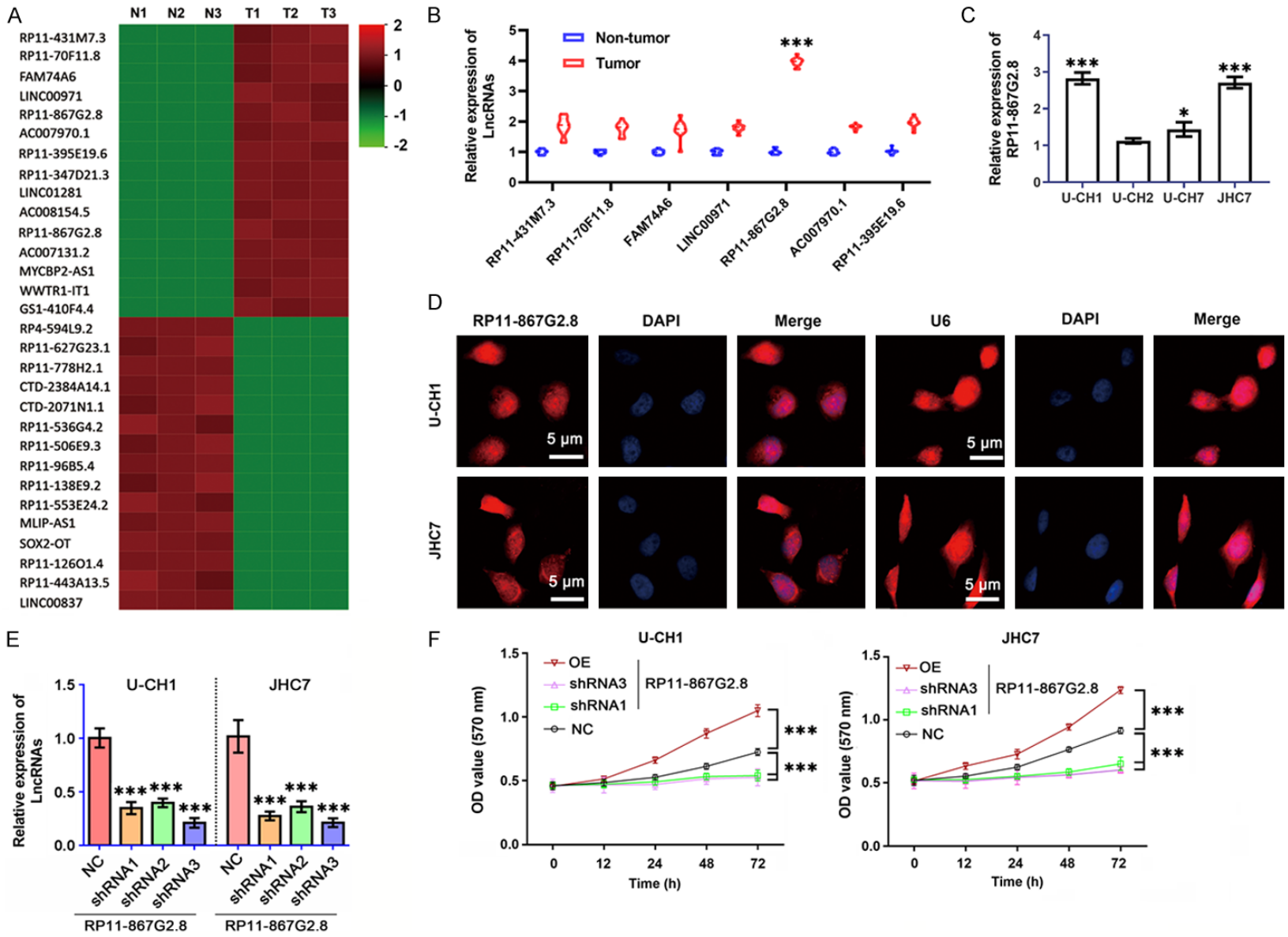
A
N1 N2 N3 T1 T2 T3
RP11-431M7.3
RP11-70F11.8
FAM74A6
LINC00971
RP11-867G2.8
AC007970.1
RP11-395E19.6
RP11-347D21.3
LINC01281
AC008154.5
RP11-867G2.8
AC007131.2
MYCBP2-AS1
WWTR1-IT1
GS1-410F4.4
RP4-594L9.2
RP11-627G23.1
RP11-778H2.1
CTD-2384A14.1
CTD-2071N1.1
RP11-536G4.2
RP11-506E9.3
RP11-96B5.4
RP11-138E9.2
RP11-553E24.2
MLIP-AS1
SOX2-OT
RP11-126O1.4
RP11-443A13.5
LINC00837
2
1
0
-1
-2
B
Relative expression of LncRNAs
Non-tumor
Tumor
***
RP11-431M7.3
RP11-70F11.8
FAM74A6
LINC00971
RP11-867G2.8
AC007970.1
RP11-395E19.6
C
Relative expression of RP11-867G2.8
***
*
***
U-CH1
U-CH2
U-CH7
JHC7
D
RP11-867G2.8
DAPI
Merge
U6
DAPI
Merge
U-CH1
JHC7
5 μm
E
Relative expression of LncRNAs
U-CH1
JHC7
***
NC
shRNA1
shRNA2
shRNA3
RP11-867G2.8
F
U-CH1
JHC7
OE
shRNA3
shRNA1
NC
RP11-867G2.8
OD value (570 nm)
Time (h)
0
12
24
48
72
***

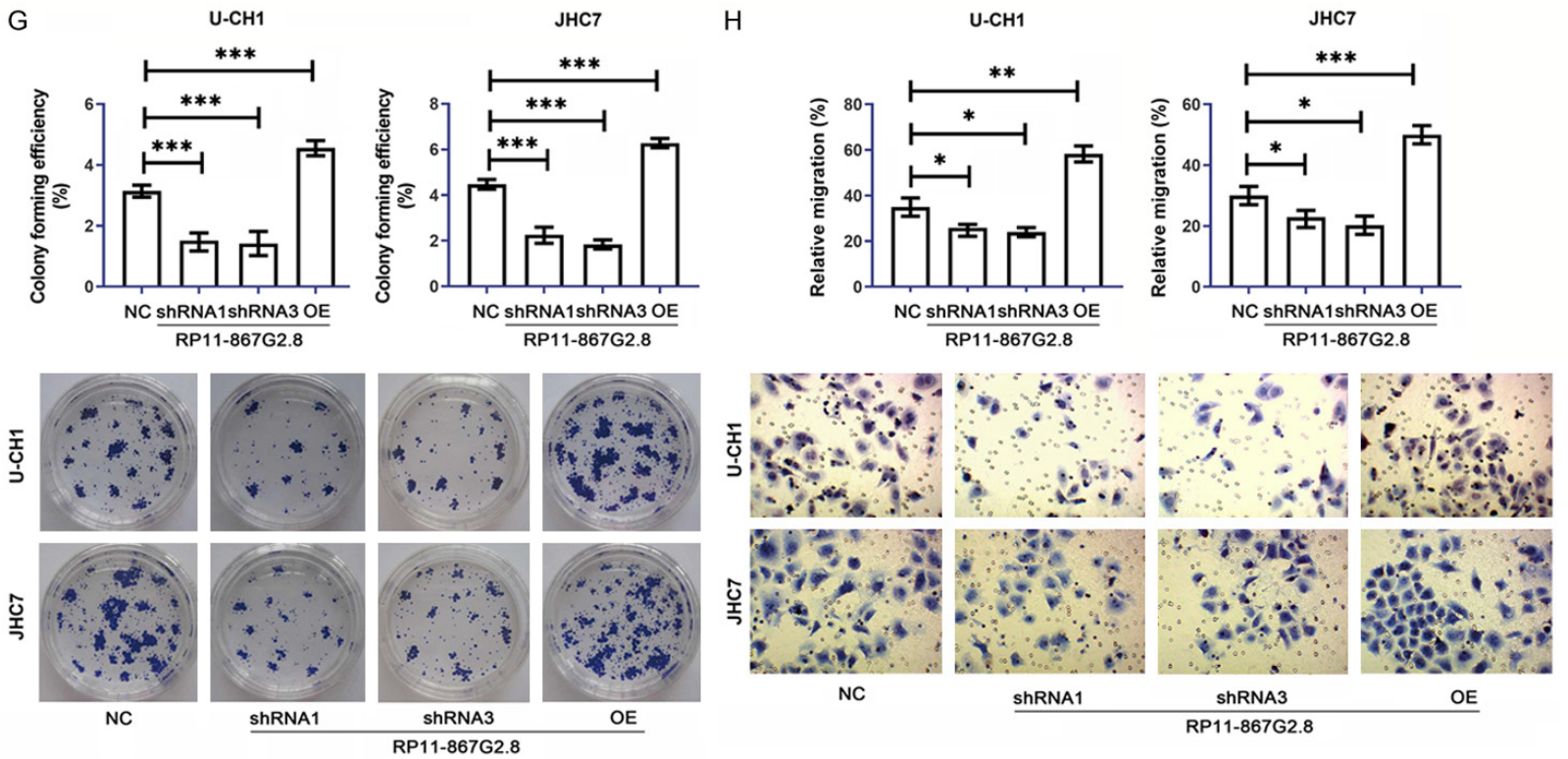

Figure 1. RP11-867G2.8 promoted the malignant biological behavior of chordoma cells. A. Heat map of the up-regulated and down-regulated lncRNAs with fold change >8. B. Expression of RP11-867G2.8 in chordoma tissues and normal nucleus pulposus tissues (n=12) by qRT-PCR. C. Expression of RP11-867G2.8 in chordoma cell lines (U-CH1, U-CH2, U-CH7 and JHC7) by qRT-PCR. D. Fluorescence in situ hybridization showed that RP11-867G2.8 was simultaneously expressed in the nucleus and cytoplasm of U-CH1 and JHC7 cells. E. We designed three shRNAs to knock down RP11-867G2.8. As indicated by the PCR, the shRNA3 showed the strongest suppressive effect on RP11-867G2.8 expression, followed by the shRNA1. F. MTT assay showed the cell proliferation of U-CH1 cells and JHC7 cells with different treatments. G. Colony formation of U-CH1 cells and JHC7 cells with different treatments. H. The transwell assay results demonstrated the cell migration of the different groups. Mean ± SD (n=3 independent experiments). $^{*}P<0.05$, $^{**}P<0.01$, $^{***}P<0.001$. Bar =10 μm.

Table 2. Bioinformatics analysis of RP11-867G2.8 (AP000943.4) as a non-coding RNA

Sequence Name	RNA Size	ORF Size	Ficket Score	Hexamer Score	Coding Probability	Coding Label
RP11-867G2.8	1038	195	0.731	0.001655	0.02311	no
FUT4	6063	1593	1.1395	0.409005	0.99999	yes
MALAT1	8779	213	0.6529	0.005321	0.01419	no

Results were obtained from the Coding Potential Assessing Tool CPAT server (http://lilab.research.bcm.edu/).

867G2.8 by shRNA1 and shRNA3. MTT results showed that the proliferation of U-CH1 and JHC7 was higher than that of the control group after overexpression of RP11-867G2.8, while lower than that of the control group after knockdown of RP11-867G2.8 (P<0.001) (**Figure 1F**). The results of colony formation showed that the clone formation rate of U-CH1 and JHC7 was higher than that of the control group after overexpression of RP11-867G2.8, and the clone formation rate of U-CH1 and JHC7 cells was lower than that of the control group after knocking down RP11-867G2.8 (P<0.001) (**Figure 1G**). Transwell results indicated that the migratory ability of U-CH1 and JHC7 cells was significantly enhanced after overexpression of RP11-867G2.8 (P<0.01, P<0.001), and the migratory ability of U-CH1 and JHC7 was lower than that of the control group after knocking down RP11-867G2.8 (P<0.05) (**Figure 1H**). These results suggested that RP11-867G2.8 promoted the proliferation and migration of chordoma cells, but the specific mechanism is still unclear.

FUT4 was highly expressed in chordoma tissues, and RP11-867G2.8 promoted the expression of FUT4

Obviously, RP11-867G2.8 overexpression changed gene transcription in chordoma cells. All the data were shown in Supplementary Table 2. A total of 16 genes were up-regulated in the transfected U-CH1 cells overexpressing RP11-867G2.8, and 18 genes were significantly down-regulated (**Figure 2A**). Results from GSEA and GO bioinformatics analysis showed that RP11-867G2.8 participated in the regulation of EMT, cell adhesion, migration, DNA-dependent transcription RNA metabolic process (**Figure 2B**, **2C**). We then further analyzed RP11-867G2.8 through the UCSC website and obtained interesting findings. The 506~1021 bp region of the fifth exon of RP11-867G2.8 was completely reversely complementary to the first exon 1482~1996 bp region of FUT4/CD15 (**Figure 2D**, **2E**). This complementary sequence suggested that RP11-867G2.8 was antisense RNA of FUT4/CD15. It has been reported that antisense RNA forms a hybrid double strand (DNA-RNA, RNA-RNA) with target gene DNA or mRNA, and promotes or inhibits transcription of a target gene or enhances the stability of a target mRNA [26, 27]. To further validate our hypothesis, we examined the protein expression level of FUT4 in 12 pairs of chordoma tissues and 12 pairs of normal nucleus pulposus tissues. The results showed that FUT4 expression level in chordoma tissues was higher than that in normal nucleus pulposus tissues (P<0.05) (**Figure 3A**). Next, we observed that RP11-867G2.8 was overexpressed in U-CH1 and JHC7 cells transfected with the full sequences of RP11-867G2.8 (P<0.001), overlapping sequence of RP11-867G2.8 and FUT4 (P<0.001), while short-hairpin RNA targeting RP11-867G2.8 elicited the down-regulation of FUT4 (P<0.001) at protein and mRNA levels (**Figure 3B-D**). In addition, RP11-NO also elevated protein expression of FUT4 (P<0.05) (**Figure 3B**). However, non-overlapping regions of RP11-867G2.8 and FUT4 conferred no effects on mRNA and protein expression of FUT4 (**Figure 3C**, **3D**). These results suggested that RP11-867G2.8 was an antisense RNA of FUT4, and RP11-867G2.8 promoted the expression of FUT4 at mRNA and protein levels. However, further studies are needed to illustrate the underlying mechanisms.

RP11-867G2.8 bound to FUT4 mRNA, increased its mRNA stability and promoted FUT4 translation

Next, we further explored the mechanism by which RP11-867G2.8 regulates FUT4 expression. RNA pull-down results showed that the enrichment of FUT4 in Bio-RP11-O group was significantly higher than that in Bio-NC group and Bio-RP11-NO group (P<0.001) (**Figure 4A**, **4B**). This result indicated that the 506~1021

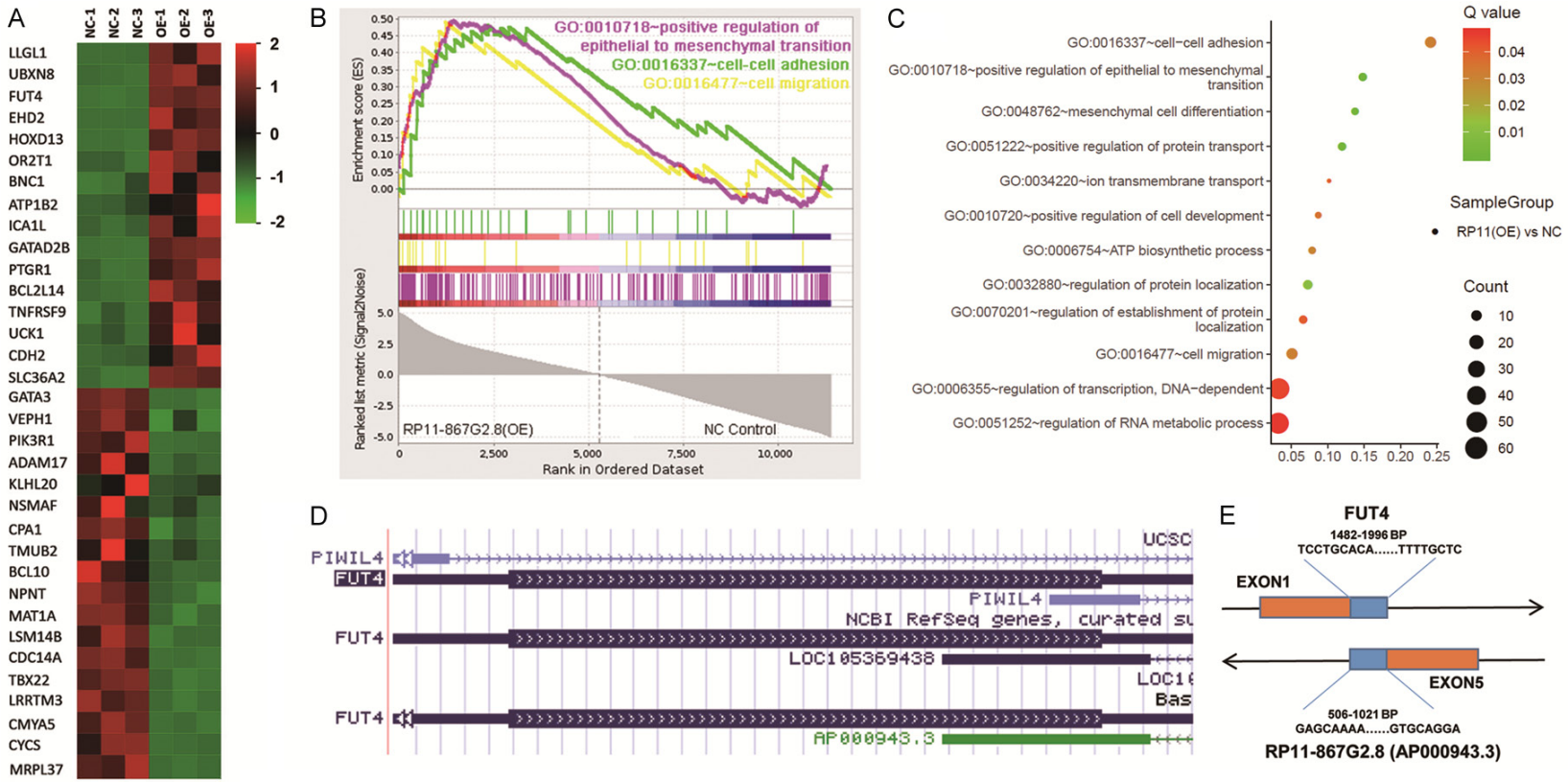

Figure 2. RPH11-867G2.8 modulated gene expression and participated in signaling transduction. (A) UCH1 cells transfected with RPH11-867G2.8 (OE) showed changes in gene transcription. (B) GSEA and (C) GO bioinformatics analyses suggested that the genes regulated by RPH11-867G2.8 possessed functions in signaling transduction. (D) UCSC analysis results showed that RP11-867G2.8 overlapped with FUT4. (E) The fifth exon partial region of RP11-867G2.8 was completely complementary to the first exon portion of FUT4.

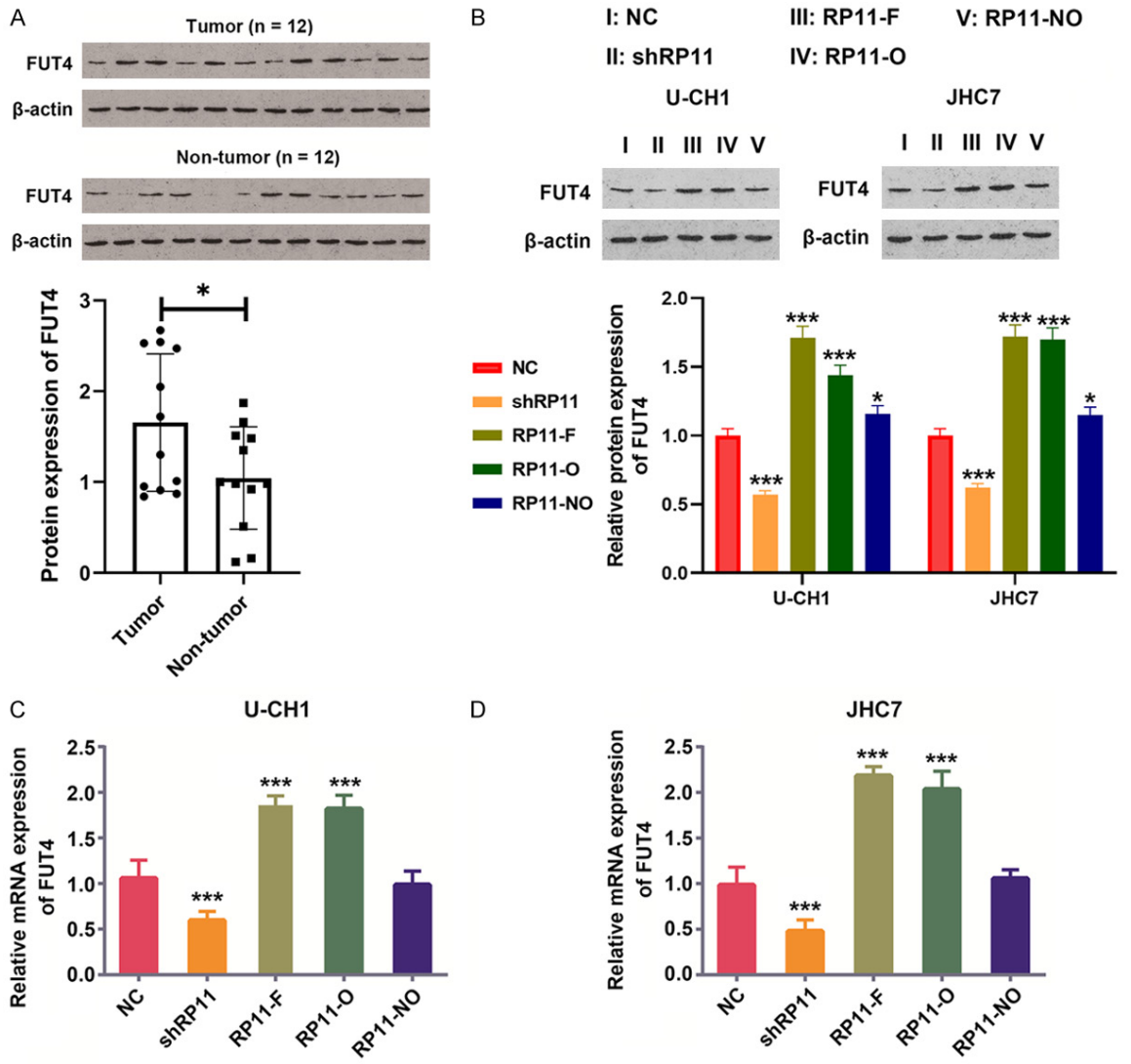

Figure 3. FUT4 was high expressed in chordoma tissues, and RP11-867G2.8 promoted the transcription of FUT4. (A) Western blot showing the protein expression of FUT4 in chordoma tissues and normal nucleus pulposus tissues. (B) Western blot showing the protein expression of FUT4 in U-CH1 and JHC7 cells transfected with the indicated plasmids. Expression of FUT4 mRNA in (C) U-CH1 and (D) JHC7 cells transfected with the indicated plasmids. NC, negative control; shRP11, short-hairpin RNA targeting RP11-867G2.8; RP11-F, full sequence of RP11-867G2.8; RP11-O, the overlapping sequence of RP11-867G2.8 with FUT4; RP11-NO, non-overlapping sequence of RP11-867G2.8 with FUT4. Mean ± SD (n=3 independent experiments). ***P<0.001.

bp region of the fifth exon of RP11-867G2.8 may directly bind to FUT4. The results of RNA stability assay showed that the half-life of FUT4 mRNA in RP11-O group was significantly longer than that of NC group, while RP11-867G2.8 knockdown contributed to a decrease in half-life of FUT4 mRNA (P<0.05, P<0.01) (**Figure 4C**, **4D**), implying that RP11-867G2.8 increased the stability of FUT4 mRNA.

Next, we used sucrose gradient centrifugation to resolve polysome fractions from cytoplasmic extracts of U-CH1 and JHC7 cells transfected with the overlapping sequence of RP11-867G2.8 and FUT4. The results showed that overexpression of RP11-867G2.8 considerably altered the polysome profile with an increase in the polysome peaks (**Figure 4E**, **4F**). Next, we used PCR and RT-PCR to examine the distribution of FUT4 mRNAs in the ribosome fractions. We found that the relative distribution of FUT4 mRNAs was shifted from sub-polysome to polysome fractions in U-CH1 and JHC7 cells transfected with RP11-867G2.8 (**Figure 4G-J**).

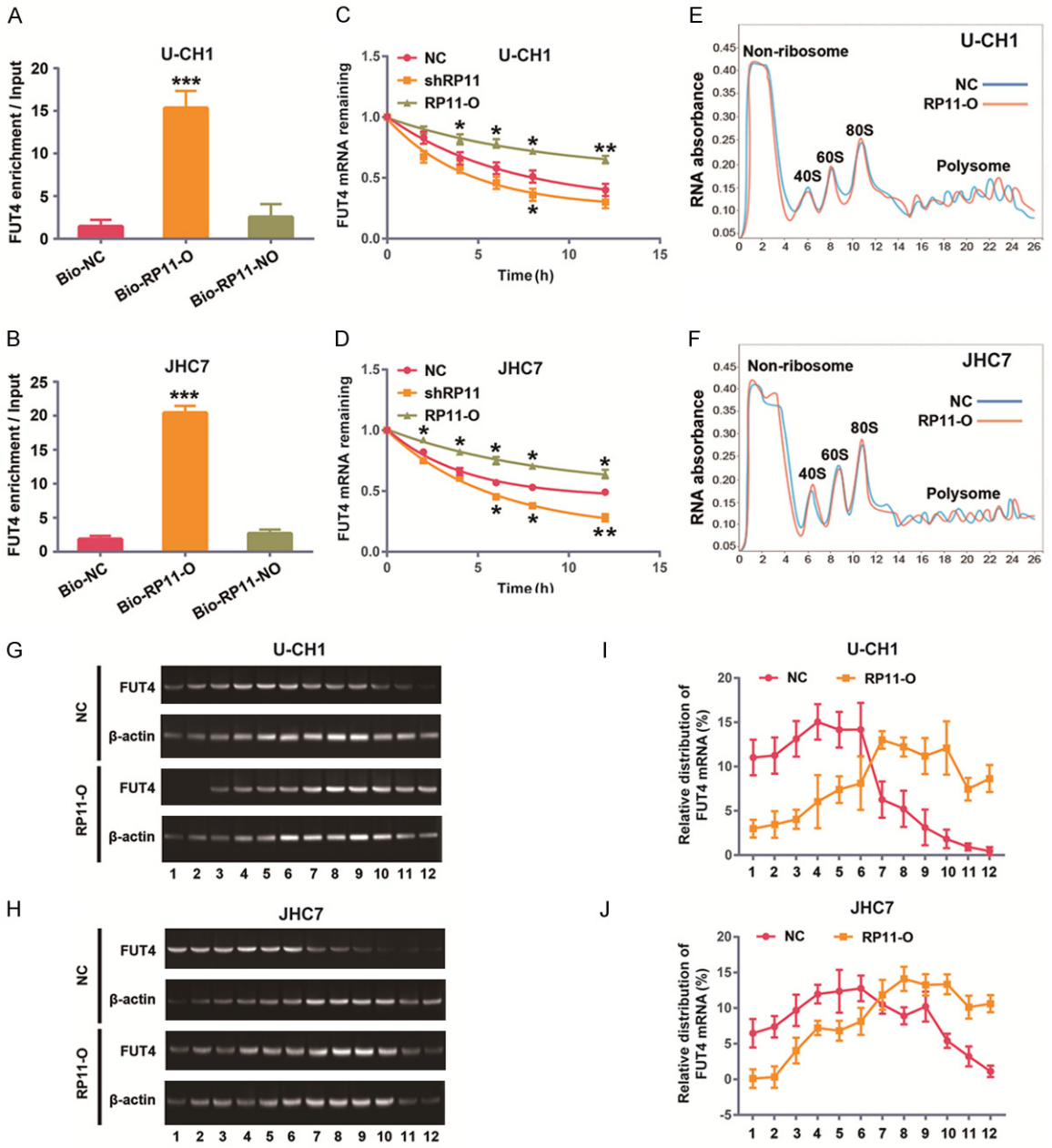

Figure 4. RP11-867G2.8 increased FUT4 mRNA stability and promoted FUT4 translation. qPCR validation of FUT4 enrichment versus input after RP11 RNA pull down using different specific probes as compared to a non-specific one in (A) U-CH1 and (B) JHC7 cells. The stability of FUT4 in transfected (C) U-CH1 and (D) JHC7 cells was measured by RT-qPCR in the presence of the transcription inhibitor Actinomycin D at the indicated time points. The half-life of FUT4 mRNA (t1/2) was calculated from each experiment shown in the graph. 18S rRNA was conducted as an internal control. (E, F) Sucrose density gradient fractionation and isolation of 40S/60S/80S and polysome cytoplasmic components for analysis, and (G, H) then polysome-fractionated samples analyzed by PCR. (I, J) Relative levels of FUT4 mRNAs in each ribosome fraction were quantified and normalized to RCN2 mRNA and plotted as a percentage of the total. Line 1-6, 40S/60S/80S; Line 7-12, polysome. NC, negative control; shRP11, short-hairpin RNA targeting RP11-867G2.8; RP11-F, full sequence of RP11-867G2.8; RP11-O, the overlapping sequence of RP11-867G2.8 with FUT4; RP11-NO, non-overlapping sequence of RP11-867G2.8 with FUT4. Data are from three independent polysome-profiling experiments. Mean ± SD (n=3 independent experiments). $^{*}P<0.05$, $^{**}P<0.01$, $^{***}P<0.001$.

This indicated that overexpression of RP11-867G2.8 promoted the translational activity of FUT4. The above results revealed that RP11-867G2.8 directly bound to FUT4 and increased

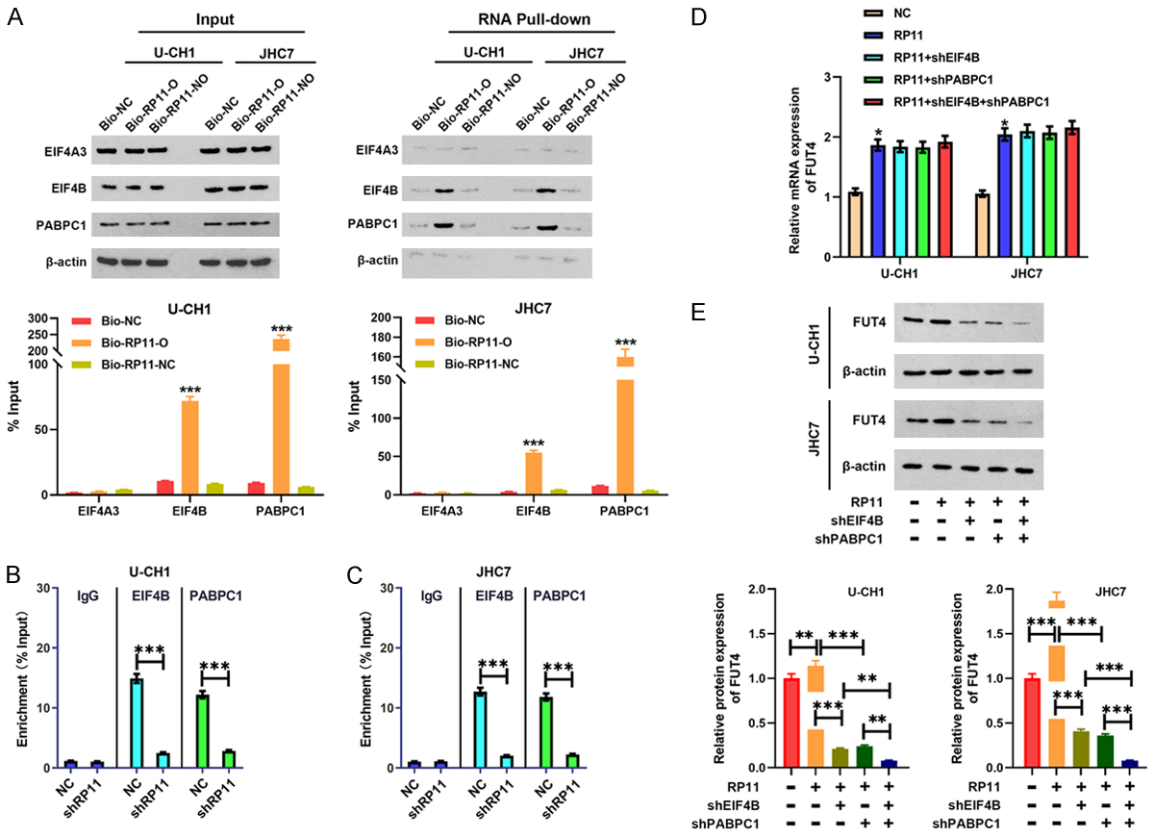

Figure 5. RP11-867G2.8 modulated FUT4 expression by recruiting EIF4B and PABPC1. (A) RNA pull-down suggested that RP11 bound to EIF4B and PABPC1 in U-CH1 and JHC7 cells. RNA immunoprecipitation experiment using antibodies against EIF4B and PABPC1 to immunoprecipitate RP11-867G2.8 from extracts of (B) U-CH1 and (C) JHC7 cells, followed by qRT-PCR quantification. (D) qRT-PCR and (E) Western blot analysis for FUT4 in U-CH1 and JHC7 cells transfected with the indicated plasmids. NC, negative control; shRP11, short-hairpin RNA targeting RP11-867G2.8; RP11, full sequence of RP11-867G2.8; RP11-O, the overlapping sequence of RP11-867G2.8 with FUT4; RP11-NO, non-overlapping sequence of RP11-867G2.8 with FUT4. Mean ± SD (n=3 independent experiments). ***P<0.001.

the stability of its mRNA, prolonged its half-life, and then promoted the translational activity of FUT4.

We analyzed the proteins that probably bind to RP11-867G2.8 using several bioinformatics analysis, including Catrapid (http://service.tartaglialab.com/page/catrapid_group), RNAct (https://rnact.crg.eu/) and RPISeq (http://pridb.gdcb.iastate.edu/RPISeq/). Among these proteins, we noticed EIF4B and PABPC1 as their showed high possibility to bind to RP11-867G2.8 (Supplementary Figure 1B). In addition, EIF4B and PABPC1 are well known for their ability to promote protein translation, therefore it is possible that RP11-867G2.8 can also regulate the translation of FUT4 mRNA by recruiting EIF4B and PABPC1. To confirm this conjecture, we chose EIF4B and PABPC1 for further study. Results from RNA pull-down showed that the overlapping sequence of RP11-867G2.8 and FUT4 mRNA bound to EIF4B and PABPC1 (P<0.001) (**Figure 5A**), which was further confirmed by RNA immunoprecipitation, that is, the enrichment of RP11-867G2.8 was obviously decreased in the complex immunoprecipitated by the antibodies against EIF4B or PABPC1 when RP11-867G2.8 was silenced in U-CH1 and JHC7 cells (P< 0.001) (**Figure 5B**, **5C**). Next, EIF4B- and PABPC1-deficient cells were constructed to confirm that EIF4B and PABPC1 are involved in the modulation of FUT4 expression. As shown in **Figure 5D**, EIF4B and PABPC1 silence showed no significant effects on FUT4 mRNA level in RP11-overexpressed U-CH1 and JHC7 cells. However, the protein expression of FUT4 was significantly decreased by shEIF4B and

shPABPC1 (P<0.01, P<0.001) (**Figure 5E**). The obtained results implied that RP11-867G2.8 may modulate FUT4 protein expression by recruiting EIF4B and PABPC1 to FUT4 mRNA.

RP11-867G2.8 promoted the malignant phenotype of chordoma cells via FUT4

The above results indicated that RP11-867G2.8 was highly expressed in chordoma tissues and cells, and RP11-867G2.8 up-regulation promoted the malignant phenotype of chordoma cells. What's more, RP11-876G2.8 increased the stability of FUT4 mRNA and promoted its translation. Based on these findings, we wondered whether RP11-c-induced up-regulation of FUT4 is associated with the effects of RP11-867G2.8 on malignant phenotype of chordoma cells. MTT results showed that overexpression of RP11-867G2.8 promoted the proliferation of chordoma cells in U-CH1 and JHC7 cells, while FUT4 silence decreased the proliferation ability (P<0.05, P<0.01) (**Figure 6A**, **6B**). The results of colony formation assay showed that overexpression of RP11-867G2.8 increased the colony formation rate of chordoma cells, while the clone formation rate of RP11 + shFUT4 group was lower than that of RP11 group (P<0.001) (**Figure 6C**, **6D**). Transwell results showed that overexpression of RP11-867G2.8 increased the migratory ability of chordoma cells, while inhibition of FUT4 expression antagonized the role of RP11-867G2.8 (P<0.01, P<0.001) (**Figure 6E**, **6F**). It has been previously reported in the literature that FUT4 has the function of an oncogene and is associated with EMT. Western blot assay results showed that the expression levels of vimentin and N-cadherin in U-CH1 and JHC7 cells transfected with RP11-867G2.8 were significantly higher than those of the control group, while the expression levels of vimentin and N-cadherin were significantly decreased when FUT4 was silenced (P<0.001) (**Figure 6G**, **6H**). All abovementioned results indicated that RP11-867G2.8 promoted proliferation, migration and EMT in chordoma cells by up-regulating FUT4.

RP11-867G2.8 promoted the progression of chordoma in vivo

Subsequently, we confirmed the synergetic functions of RP11-867G2.8 and FUT4 on chordoma *in vivo*. The results showed that the tumor volume of the mice in RP11 group was significantly larger than that of the other three groups, while the tumor volume of shRP11 and RP11 + shFUT4 groups was significantly smaller than that of the control group and the shRP11 group (P<0.05, P<0.01, P<0.001) (**Figure 7A**, **7B**). The expression of FUT4 in tumor tissues was detected by Western blot. The results showed that the protein expression of FUT4 in RP11 group was obviously increased compared to that of NC group. However, the expression levels of FUT4 in shRP11 and RP11 + shFUT4 groups were significantly reduced (P<0.05, P<0.001) (**Figure 7C**). Then IHC was used to detect the expression level of Ki67 in tumor tissues. The results showed that the expression level of Ki67 in RP11 group was significantly higher than that in the other three groups, while the expression of Ki67 in shRP11 and RP11 + shFUT4 groups was lower than that of the control group and RP11 group (**Figure 7D**). The above results demonstrated that RP11-867G2.8 may promote the progression of chordoma by up-regulating the expression of FUT4 *in vivo*.

Discussion

Dysregulated expression of lncRNAs is frequently observed in various cancers, where they act as tumor suppressors or oncogenes [28-30]. However, there is no related study about RP11-867G2.8 in chordoma. The aim of this study was to explore the function of RP11-867G2.8 and associated mechanism in chordoma.

Our results indicated that RP11-867G2.8 was highly expressed in chordoma tissues and cells, and overexpression of RP11-867G2.8 promoted the malignant biological behavior of chordoma cells, indicating that RP11-867G2.8 is an oncogene in chordoma. Results from fluorescence in situ hybridization assay showed that RP11-867G2.8 was simultaneously expressed in the nucleus and cytoplasm, which means that RP11-867G2.8 can regulate the malignant biological behavior of chordoma cells through various pathways. There have been many studies on lncRNA down-regulating miRNA through ceRNA mechanism to play a general purpose [31, 32], but this indirect mechanism often has limited effects, and no similar results can be applied in practice. Therefore, we are eager to find a more direct

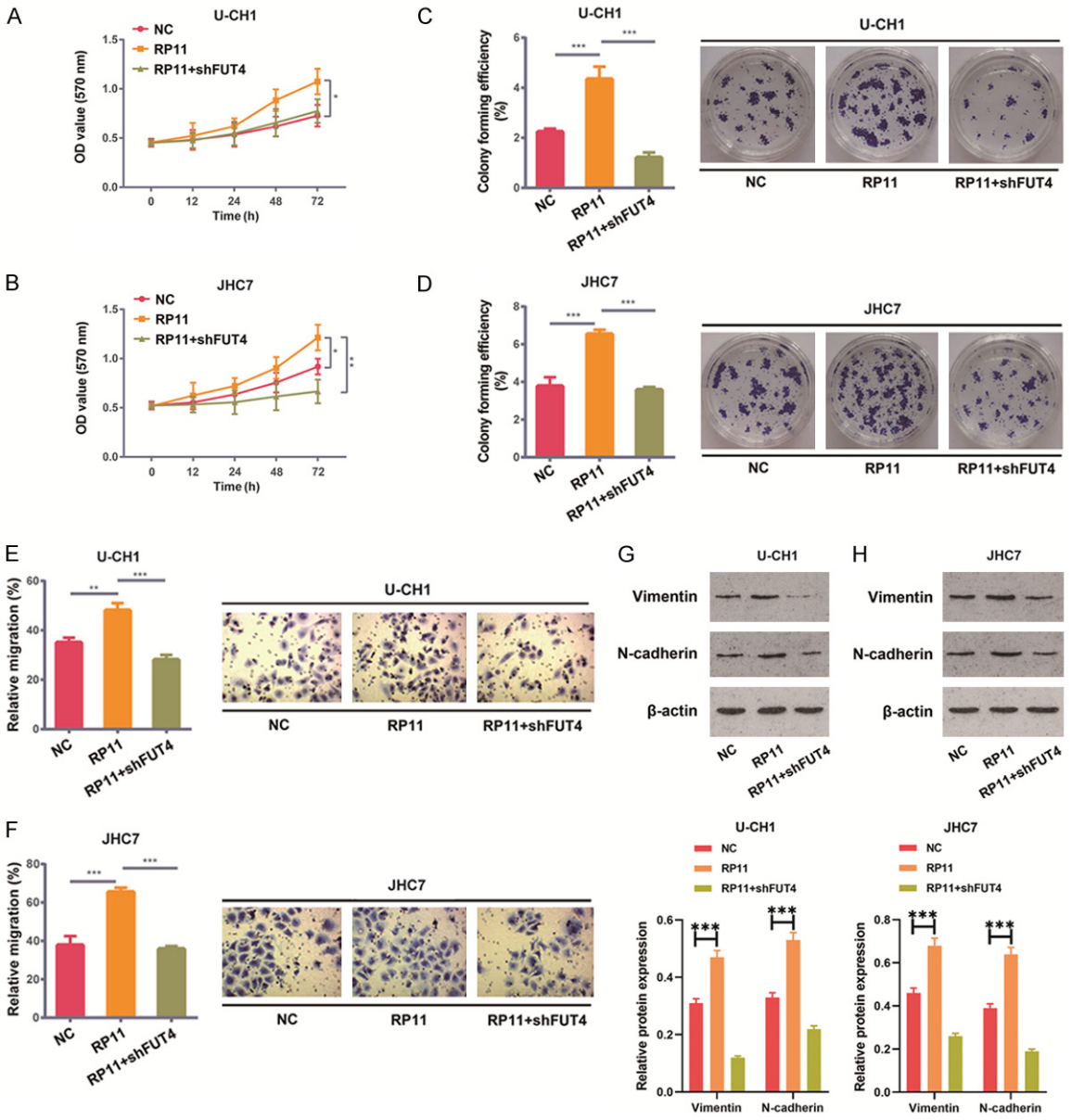

Figure 6. RP11-867G2.8 promoted the malignant phenotype of chordoma cells via FUT4. MTT assay showing the cell proliferation of (A) U-CH1 cells and (B) JHC7 cells transfected with the indicated plasmids. Colony formation of (C) U-CH1 cells and (D) JHC7 cells with different treatments. The transwell assay results demonstrated the migratory activities of (E) U-CH1 and (F) JHC7 cells transfected with the indicated plasmids. Epithelial-mesenchymal transition (EMT) related markers vimentin and N-cadherin in (G) U-CH1 and (H) JHC7 cells transfected with the indicated plasmids were detected by Western blot. NC, negative control; RP11, full sequence of RP11-867G2.8; shFUT4, short-hairpin RNA targeting FUT4. Mean ± SD (n=3 independent experiments). $^{*}P<0.05$, $^{**}P<0.01$, $^{***}P<0.001$.

mechanism to explain the effects of RP11, such as directly binding to proteins or directly acting on functional genes [33].

In further searching for the downstream molecules of RP11, a new discovery caught our attention. The fifth exon of RP11 is completely complementary to the first exon (1482-1996 bp) of FUT4. FUT4/CD15 has the function of oncogene. It has been reported that FUT4 can participate in the regulation of cell proliferation, differentiation and EMT [18-21]. However, the function of FUT4 in chordoma is still unclear. In the current reports, antisense RNA

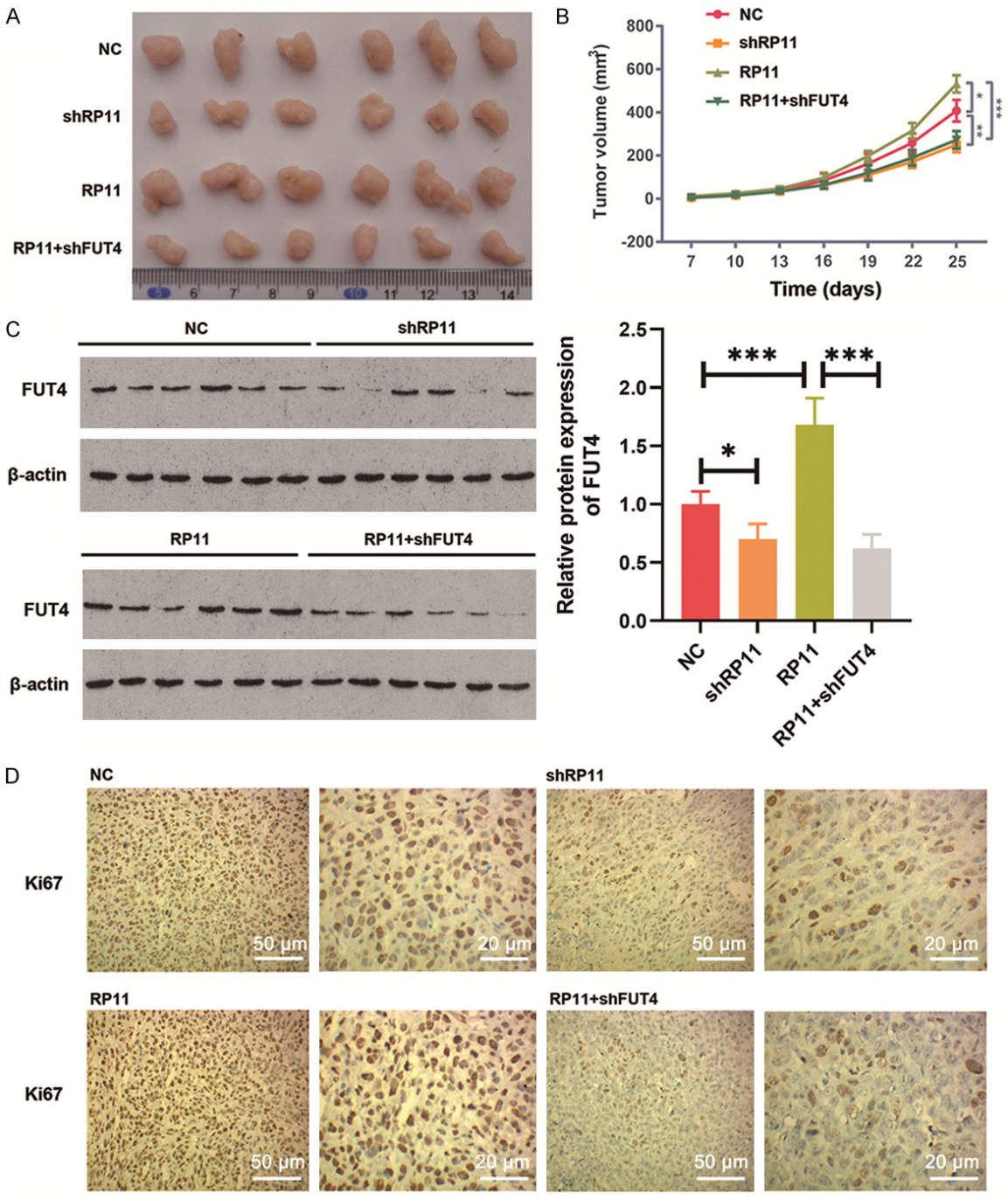

Figure 7. RP11-867G2.8 promoted the progression of chordoma *in vivo*. A. Tumor tissues isolated from indicated mice at day 25 post-transplant. B. Tumor growth curve in nude mice. U-CH1 cells transfected with the indicated plasmids were injected subcutaneously into the right flank of the abdomen of nude mice, the short and long diameters of the tumors were measured every 3 days and tumor volumes (mm^3) were calculated. C. Expression of FUT4 protein in U-CH1 xenografts. D. Immunohistochemistry showing the Ki67 expression of U-CH1 xenografts. NC, negative control; RP11, full sequence of RP11-867G2.8; shRP11, short-hairpin RNA targeting RP11-867G2.8; shFUT4, short-hairpin RNA targeting FUT4. Mean ± SD (n=3 independent experiments). $^{*}P<0.05$, $^{**}P<0.01$, $^{***}P<0.001$.

mainly plays a two-way role. Antisense transcripts combines with the target sense gene to form a complementary double strand, which may promote or inhibit gene transcription, and may also maintain the stability of the target gene and promote protein translation [26, 27].

Therefore, we consider that RP11-867G2.8 may regulate the expression of FUT4 by forming a double strand with it. Subsequent experiments further verified our hypothesis. The RNA stability assay and the polysome fractionation test proved that the overlapping area of RP11-867G2.8 and FUT4 can promote the mRNA stability of FUT4 and promote the translation of FUT4 protein. This means that FUT4 is very likely to be an oncogene in chordoma, which is consistent with reports of FUT4 in other tumors.

In addition, this discovery raises our question, that is, whether FUT4 also promotes RP11-867G2.8 mRNA stability and whether FUT4 promotes the malignant phenotype of chordoma by promoting the stability of RP11 mRNA. We think this is a question worthy of in-depth consideration and research. Interestingly, we found that RP11-867G2.8 bound to EIF4B and PABPC1. What's more, EIF4B and PABPC1 down-regulation was found to decrease the translation of FUT4. Translation initiation occurs at which the ribosome is recruited to the mRNA, and EIFs like EIF4B are involved in this process [34]. PABPC1 offers positional information discriminating premature from natural stops that trigger nonsense-mediated mRNA decay, and then shows roles in mRNA surveillance [35]. What's more, the online website catRAPID was used to predict the binding region of protein and RNA. The obtained results revealed that the potential binding region of PABPC1 and EIF4B with RP11-867G2.8 is the overlapping sequence of RP11-OL and FUT4.

In the next study, we demonstrated through cell and animal experiments that RP11-867G2.8 promotes the progression of chordoma by up-regulating the expression of FUT4. RP11-867G2.8 may promote proliferation and migration of chordoma cells through increasing the stability of FUT4 mRNA. However, it is worth mentioning that FUT4 is also a molecular marker of stem cells [36-38]. Therefore, RP11-867G2.8 is also very likely to affect the differentiation and self-renewal of chordate stem cells. We will further explore the correlation between RP11-867G2.8 and chordoma stem cells in future studies.

Conclusions

In the present study, we found that RP11-867G2.8 is a natural antisense RNA of FUT4, and RP11-867G2.8 can directly bind to FUT4 to form a double strand to increase the stability of FUT4 mRNA and promote its translation. RP11-876G2.8 promotes the progression of chordoma by up-regulating the expression of FUT4. However, RP11-867G2.8 may have more functions and mechanisms that require us to explore further.

Acknowledgements

This publication was funded by Natural Science Foundation of the Department of Science and Technology of Shanxi province (2019JM-200); Social Development Science Foundation of the Department of Science and Technology of ShanXi province (2021SF-248).

Disclosure of conflict of interest

None.

Address correspondence to: Zhong Kai Liu and Xin Hua Yin, Department of Spine Surgery, Hong Hui Hospital, Xi'an Jiaotong University College of Medicine, No. 555, East Youyi Road, Xi'an, Shaanxi, China. E-mail: spine2020@sina.com (ZKL); mangiferia@sina.com (XHY)

References

[1] McMaster ML, Goldstein AM, Bromley CM, Ishibe N and Parry DM. Chordoma: incidence and survival patterns in the United States, 1973-1995. Cancer Causes Control 2001; 12: 1-11.

[2] Chambers KJ, Lin DT, Meier J, Remenschneider A, Herr M and Gray ST. Incidence and survival patterns of cranial chordoma in the United States. Laryngoscope 2014; 124: 1097-1102.

[3] Yu E, Koffer PP, DiPetrillo TA and Kinsella TJ. Incidence, treatment, and survival patterns for sacral chordoma in the United States, 1974-2011. Front Oncol 2016; 6: 203.

[4] Almefty K, Pravdenkova S, Colli BO, Al-Mefty O and Gokden M. Chordoma and chondrosarcoma: similar, but quite different, skull base tumors. Cancer 2007; 110: 2457-2467.

[5] Gagliardi F, Boari N, Riva P and Mortini P. Current therapeutic options and novel molecular markers in skull base chordomas. Neurosurg Rev 2012; 35: 1-13.

[6] Catton C, O'Sullivan B, Bell R, Laperriere N, Cummings B, Fornasier V and Wunder J. Chordoma: long-term follow-up after radical photon irradiation. Radiother Oncol 1996; 41: 67-72.

[7] Osaka S, Kodoh O, Sugita H, Osaka E, Yoshida Y and Ryu J. Clinical significance of a wide excision policy for sacrococcygeal chordoma. J Cancer Res Clin Oncol 2006; 132: 213-218.
[8] Lin C and Yang L. Long noncoding RNA in cancer: wiring signaling circuitry. Trends Cell Biol 2018; 28: 287-301.
[9] Quinn JJ and Chang HY. Unique features of long non-coding RNA biogenesis and function. Nat Rev Genet 2016; 17: 47-62.
[10] Thomson DW and Dinger ME. Endogenous microRNA sponges: evidence and controversy. Nat Rev Genet 2016; 17: 272-283.
[11] van Heesch S, van Iterson M, Jacobi J, Boymans S, Essers PB, de Bruijn E, Hao W, MacInnes AW, Cuppen E and Simonis M. Extensive localization of long noncoding RNAs to the cytosol and mono- and polyribosomal complexes. Genome Biol 2014; 15: R6.
[12] Schmitt AM and Chang HY. Long noncoding RNAs in cancer pathways. Cancer Cell 2016; 29: 452-463.
[13] Wang Y, Zhong H, Xie X, Chen CY, Huang D, Shen L, Zhang H, Chen ZW and Zeng G. Long noncoding RNA derived from CD244 signaling epigenetically controls CD8+ T-cell immune responses in tuberculosis infection. Proc Natl Acad Sci U S A 2015; 112: E3883-3892.
[14] Shih JW, Chiang WF, Wu ATH, Wu MH, Wang LY, Yu YL, Hung YW, Wang WC, Chu CY, Hung CL, Changou CA, Yen Y and Kung HJ. Long noncoding RNA LncHIFCAR/MIR31HG is a HIF-1α coactivator driving oral cancer progression. Nat Commun 2017; 8: 15874.
[15] Xu N, Liu B, Lian C, Doycheva DM, Fu Z, Liu Y, Zhou J, He Z, Yang Z, Huang Q, Zeng H and Guo H. Long noncoding RNA AC003092.1 promotes temozolomide chemosensitivity through miR-195/TFPI-2 signaling modulation in glioblastoma. Cell Death Dis 2018; 9: 1139.
[16] Ma X, Qi S, Duan Z, Liao H, Yang B, Wang W, Tan J, Li Q and Xia X. Long non-coding RNA LOC554202 modulates chordoma cell proliferation and invasion by recruiting EZH2 and regulating miR-31 expression. Cell Prolif 2017; 50: e12388.
[17] Chen H, Zhang K, Lu J, Wu G, Yang H and Chen K. Comprehensive analysis of mRNA-lncRNA co-expression profile revealing crucial role of imprinted gene cluster DLK1-MEG3 in chordoma. Oncotarget 2017; 8: 112623-112635.
[18] Yang X, Liu S and Yan Q. Role of fucosyltransferase IV in epithelial-mesenchymal transition in breast cancer cells. Cell Death Dis 2013; 4: e735.
[19] Giordano G, Febbraro A, Tomaselli E, Sarnicola ML, Parcesepe P, Parente D, Forte N, Fabozzi A, Remo A, Bonetti A, Manfrin E, Ghasemi S, Ceccarelli M, Cerulo L, Bazzoni F and Pancione M. Cancer-related CD15/FUT4 overexpression decreases benefit to agents targeting EGFR or VEGF acting as a novel RAF-MEK-ERK kinase downstream regulator in metastatic colorectal cancer. J Exp Clin Cancer Res 2015; 34: 108.
[20] Liu B, Ma H, Liu Q, Xiao Y, Pan S, Zhou H and Jia L. MiR-29b/Sp1/FUT4 axis modulates the malignancy of leukemia stem cells by regulating fucosylation via Wnt/beta-catenin pathway in acute myeloid leukemia. J Exp Clin Cancer Res 2019; 38: 200.
[21] Li Y, Sun Z, Liu B, Shan Y, Zhao L and Jia L. Tumor-suppressive miR-26a and miR-26b inhibit cell aggressiveness by regulating FUT4 in colorectal cancer. Cell Death Dis 2017; 8: e2892.
[22] Huang H, Weng H, Sun W, Qin X, Shi H, Wu H, Zhao BS, Mesquita A, Liu C, Yuan CL, Hu YC, Huttelmaier S, Skibbe JR, Su R, Deng X, Dong L, Sun M, Li C, Nachtergaele S, Wang Y, Hu C, Ferchen K, Greis KD, Jiang X, Wei M, Qu L, Guan JL, He C, Yang J and Chen J. Recognition of RNA N(6)-methyladenosine by IGF2BP proteins enhances mRNA stability and translation. Nat Cell Biol 2018; 20: 285-295.
[23] Conrad NK, Mili S, Marshall EL, Shu MD and Steitz JA. Identification of a rapid mammalian deadenylation-dependent decay pathway and its inhibition by a viral RNA element. Mol Cell 2006; 24: 943-953.
[24] Kim KM, Cho H, Choi K, Kim J, Kim BW, Ko YG, Jang SK and Kim YK. A new MIF4G domain-containing protein, CTIF, directs nuclear cap-binding protein CBP80/20-dependent translation. Genes Dev 2009; 23: 2033-2045.
[25] Lin S, Choe J, Du P, Triboulet R and Gregory RI. The m(6)A methyltransferase METTL3 promotes translation in human cancer cells. Mol Cell 2016; 62: 335-345.
[26] Faghihi MA, Modarresi F, Khalil AM, Wood DE, Sahagan BG, Morgan TE, Finch CE, St Laurent G 3rd, Kenny PJ and Wahlestedt C. Expression of a noncoding RNA is elevated in Alzheimer's disease and drives rapid feed-forward regulation of beta-secretase. Nat Med 2008; 14: 723-730.
[27] Huang B, Song JH, Cheng Y, Abraham JM, Ibrahim S, Sun Z, Ke X and Meltzer SJ. Long noncoding antisense RNA KRT7-AS is activated in gastric cancers and supports cancer cell progression by increasing KRT7 expression. Oncogene 2016; 35: 4927-4936.
[28] Liu J, Ben Q, Lu E, He X, Yang X, Ma J, Zhang W, Wang Z, Liu T, Zhang J and Wang H. Long noncoding RNA PANDAR blocks CDKN1A gene transcription by competitive interaction with p53 protein in gastric cancer. Cell Death Dis 2018; 9: 168.

[29] Sun Y, Hu B, Wang Q, Ye M, Qiu Q, Zhou Y, Zeng F, Zhang X, Guo Y and Guo L. Long non-coding RNA HOTTIP promotes BCL-2 expression and induces chemoresistance in small cell lung cancer by sponging miR-216a. Cell Death Dis 2018; 9: 85.

[30] Wang S, Liang K, Hu Q, Li P, Song J, Yang Y, Yao J, Mangala LS, Li C, Yang W, Park PK, Hawke DH, Zhou J, Zhou Y, Xia W, Hung MC, Marks JR, Gallick GE, Lopez-Berestein G, Flores ER, Sood AK, Huang S, Yu D, Yang L and Lin C. JAK2-binding long noncoding RNA promotes breast cancer brain metastasis. J Clin Invest 2017; 127: 4498-4515.

[31] Li FP, Lin DQ and Gao LY. LncRNA TUG1 promotes proliferation of vascular smooth muscle cell and atherosclerosis through regulating miRNA-21/PTEN axis. Eur Rev Med Pharmacol Sci 2018; 22: 7439-7447.

[32] Zhao W, Geng D, Li S, Chen Z and Sun M. LncRNA HOTAIR influences cell growth, migration, invasion, and apoptosis via the miR-20a-5p/HMGA2 axis in breast cancer. Cancer Med 2018; 7: 842-855.

[33] Zhang Q, Wei Y, Yan Z, Wu C, Chang Z, Zhu Y, Li K and Xu Y. The characteristic landscape of lncRNAs classified by RBP-lncRNA interactions across 10 cancers. Mol Biosyst 2017; 13: 1142-1151.

[34] Nielsen KH, Behrens MA, He Y, Oliveira CL, Jensen LS, Hoffmann SV, Pedersen JS and Andersen GR. Synergistic activation of eIF4A by eIF4B and eIF4G. Nucleic Acids Res 2011; 39: 2678-2689.

[35] Behm-Ansmant I, Gatfield D, Rehwinkel J, Hilgers V and Izaurralde E. A conserved role for cytoplasmic poly(A)-binding protein 1 (PABPC1) in nonsense-mediated mRNA decay. EMBO J 2007; 26: 1591-1601.

[36] Singh AR, Joshi S, Zulcic M, Alcaraz M, Garlich JR, Morales GA, Cho YJ, Bao L, Levy ML, Newbury R, Malicki D, Messer K, Crawford J and Durden DL. PI-3K inhibitors preferentially target CD15+ cancer stem cell population in SHH driven medulloblastoma. PLoS One 2016; 11: e0150836.

[37] Lukenda A, Dotlic S, Vukojevic N, Saric B, Vranic S and Zarkovic K. Expression and prognostic value of putative cancer stem cell markers CD117 and CD15 in choroidal and ciliary body melanoma. J Clin Pathol 2016; 69: 234-239.

[38] Kahlert UD, Bender NO, Maciaczyk D, Bogiel T, Bar EE, Eberhart CG, Nikkhah G and Maciaczyk J. CD133/CD15 defines distinct cell subpopulations with differential in vitro clonogenic activity and stem cell-related gene expression profile in in vitro propagated glioblastoma multiforme-derived cell line with a PNET-like component. Folia Neuropathol 2012; 50: 357-368.

A

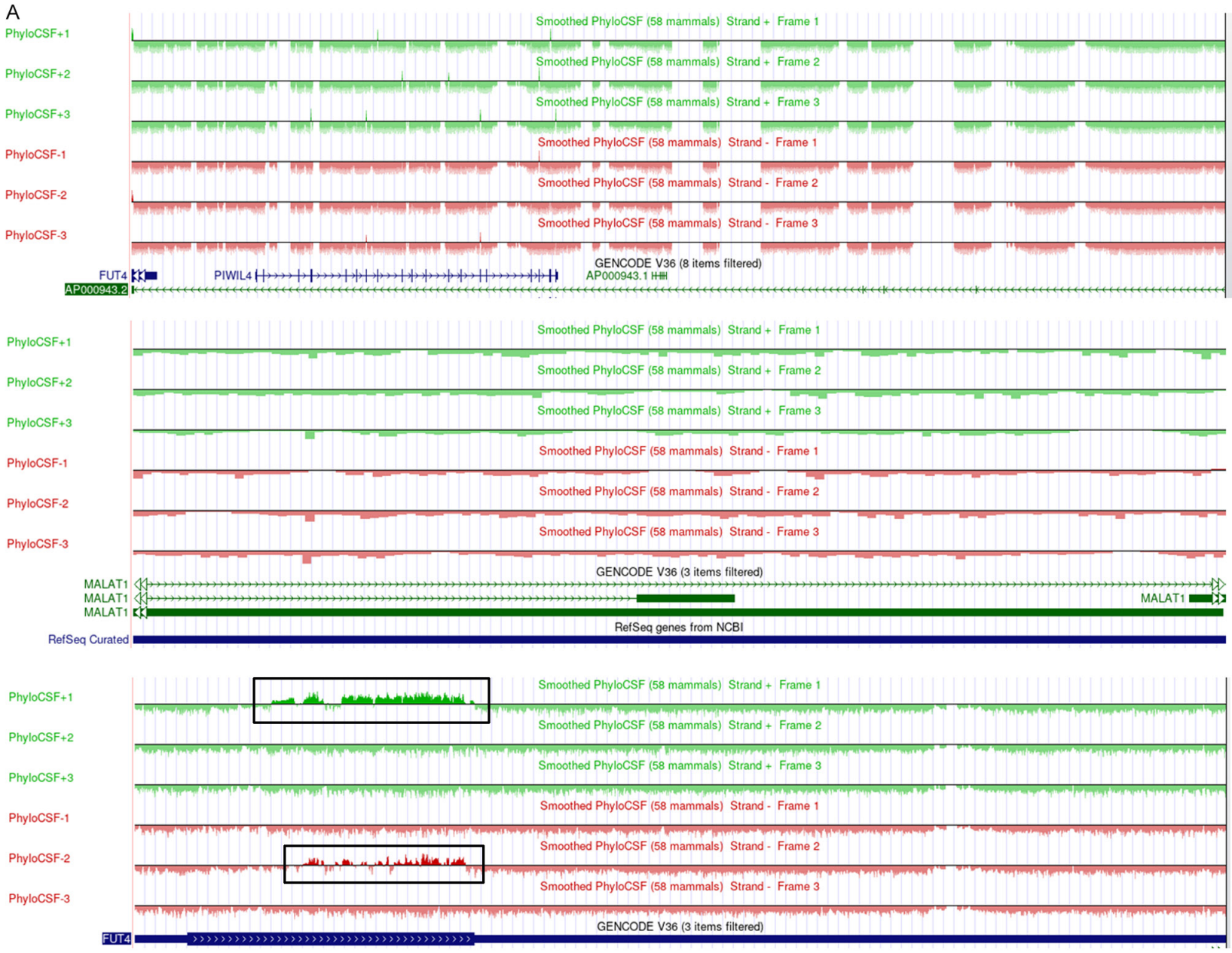
PhyloCSF+1
PhyloCSF+2
PhyloCSF+3
PhyloCSF-1
PhyloCSF-2
PhyloCSF-3
Smoothed PhyloCSF (58 mammals) Strand + Frame 1
Smoothed PhyloCSF (58 mammals) Strand + Frame 2
Smoothed PhyloCSF (58 mammals) Strand + Frame 3
Smoothed PhyloCSF (58 mammals) Strand - Frame 1
Smoothed PhyloCSF (58 mammals) Strand - Frame 2
Smoothed PhyloCSF (58 mammals) Strand - Frame 3
FUT4
PIWIL4
AP000943.2
GENCODE V36 (8 items filtered)
AP000943.1
MALAT1
GENCODE V36 (3 items filtered)
RefSeq Curated
RefSeq genes from NCBI

B

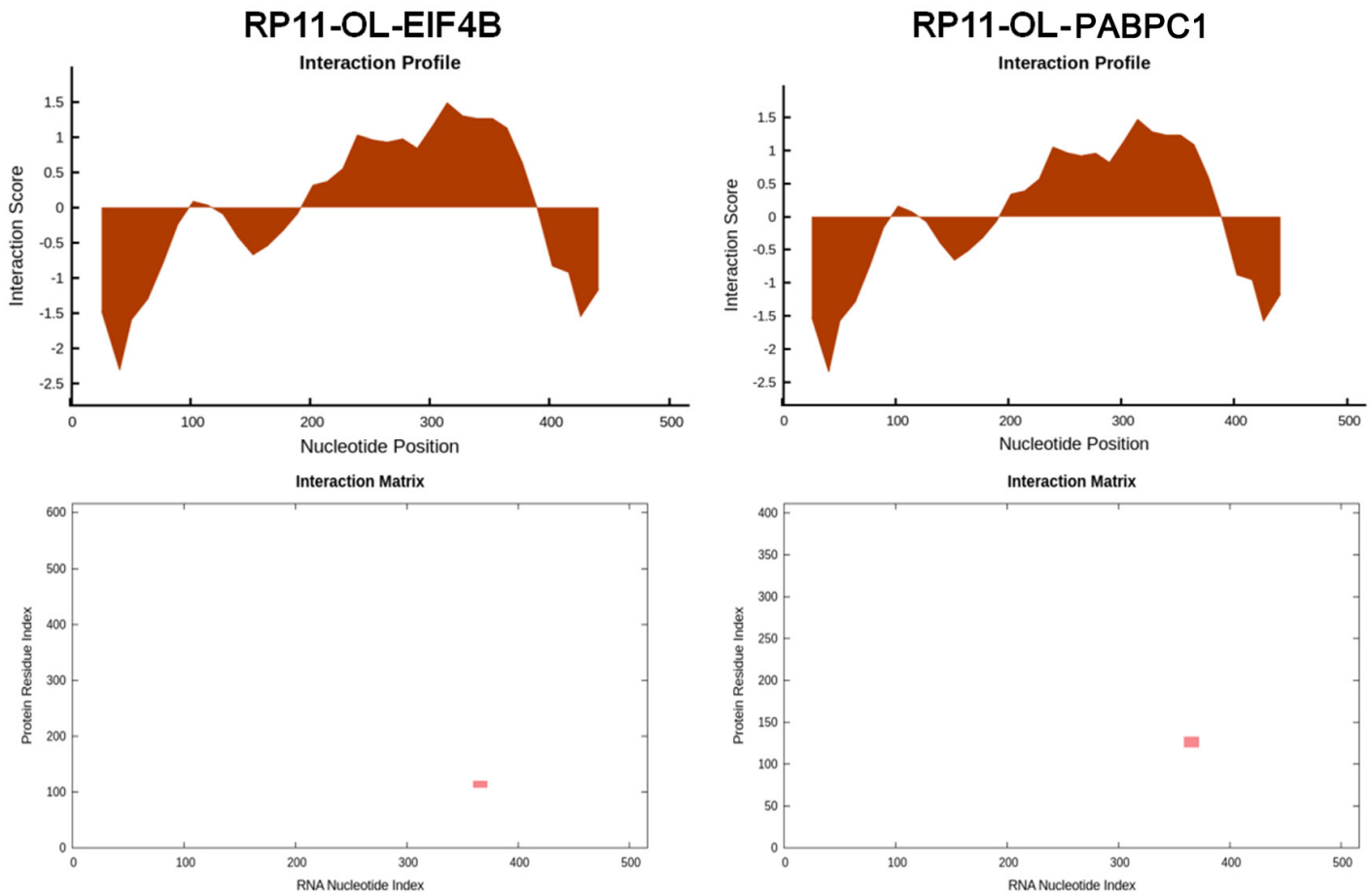

Supplementary Figure 1. The prediction of coding region of RNA and the analysis of RP11-867G2.8 binding to EIF4B and PABPC1. (A) PhyloCSF Candidate Coding Regions (https://github.com/mlin/PhyloCSF/wiki) was used to distinguish protein coding region and non coding region of RNAs, including FUT4, RP11-867G2.8 and MALAT1. The output value of PhyloCSF is more than zero, indicating a conservative coding area; otherwise, it indicates a non coding area. (B) We analyzed the proteins that probably bind to RP11-867G2.8 using bioinformatics analysis in Catrapid (http://service.tartaglialab.com/page/catrapid_group). EIF4B and PABPC1 showed high possibility to bind to RP11-867G2.8.